nature physics

LETTERS

PUBLISHED ONLINE: 26 JANUARY 2014 | DOI: 10.1038/NPHYS2880

Double ionization probed on the attosecond timescale

Erik P. Månsson[1], Diego Guénot[2], Cord L. Arnold[2], David Kroon[2], Susan Kasper[1], J. Marcus Dahlström[3], Eva Lindroth[3], Anatoli S. Kheifets[4], Anne L'Huillier[2], Stacey L. Sorensen[1] and Mathieu Gisselbrecht[1,2]*

Double ionization following the absorption of a single photon is one of the most fundamental processes requiring interaction between electrons[1–3]. Information about this interaction is usually obtained by detecting emitted particles without access to real-time dynamics. Here, attosecond light pulses[4,5], electron wave packet interferometry[6] and coincidence techniques[7] are combined to measure electron emission times in double ionization of xenon using single ionization as a clock, providing unique insight into the two-electron ejection mechanism. Access to many-particle dynamics in real time is of fundamental importance for understanding processes induced by electron correlation in atomic, molecular and more complex systems.

The emergence of attosecond science ($1\,\mathrm{as} = 10^{-18}\,\mathrm{s}$) in the new millennium opened an exciting area of physics bringing the dynamics of electron wave functions into focus. The important goal of real-time visualization of the interplay between electrons and their role in molecular bonding now seems to be in reach. After a decade where attosecond light sources[4,5] were characterized and their potential demonstrated, the next phase will include the exploration of correlated electron dynamics in complex systems. A series of ground-breaking studies on single ionization (SI) in atoms using attosecond light pulses sheds light on the escaping electron and its interaction with the residual ion[6,8], and the resulting coherent superposition of neutral bound states[9,10].

Double ionization (DI) by absorption of a single photon is an inherently more challenging phenomenon, both experimentally and theoretically[1–3]. The two-electron ejection can be understood only through interactions between electrons, and is usually discussed in terms of different mechanisms[11]. In the knockout mechanism, the electron excited by interaction with the light field (the photoelectron) collides with another electron on its way out, resulting in two emitted electrons. In the shake-off mechanism, orbital relaxation following the creation of a hole ionizes a second electron. Electron correlations may also lead to indirect DI processes via highly excited states of the singly-charged ion[12]. One-photon experimental investigations with the pair of electrons detected in coincidence can provide a fairly complete DI description without, however, following the dynamics of the electron correlation in real time. Multiphoton experimental investigations have been performed both on the femtosecond and attosecond timescales[13,14], but DI in strong laser fields does not require electron correlation.

In this work, we study DI of xenon in the near-threshold region using attosecond extreme ultraviolet (XUV) pulses for excitation and multi-electron coincidence techniques to disentangle SI and DI events. Using an interferometric technique with a weak infrared laser field, we demonstrate the existence of different ionization mechanisms and get new insight into the quantum dynamics of one-photon DI with evidence for inter-shell correlation effects.

In our experiment (Fig. 1 and Supplementary Methods) a train of attosecond pulses corresponding to a coherent comb of odd harmonics was generated by the interaction of an intense femtosecond laser with Ar gas and focused on a jet of Xe atoms. Electrons were detected in coincidence in a magnetic bottle spectrometer and their energies retrieved from their flight times. The weak dressing infrared field was collinear with the ionizing XUV field and could be delayed with attosecond precision. Interference patterns resulting from multiple infrared-induced quantum paths were studied as a function of the delay (τ) between the XUV and infrared fields.

First we consider the interaction of Xe with XUV pulses only. Figure 2a illustrates the relevant electronic structure in the vicinity of the double-ionization threshold together with measured and simulated two-electron coincidence spectra (Fig. 2b). The spectra contain horizontal stripes arising from different final states and harmonic orders. In agreement with previous work[7], we find that $^3P_2$ and $^1D_2$ are the dominant Xe^{2+} final states. In each stripe the electron pair exhibits both a continuous energy distribution characteristic of direct DI and discrete peaks due to indirect processes. The simulation uses spectroscopic data[7,15,16] and takes into account our experimental parameters (see Supplementary Methods). The excellent agreement between experimental and simulated spectra allows us to unambiguously identify the majority of the observed features.

The infrared field required for our interferometric measurement opens new processes for two-electron ejection[17–21]. Ionization takes place in a 'non-sequential' process with the absorption of two photons from the atomic ground state or via a 'sequential' process, where the XUV photon is absorbed by the neutral atom, and the infrared photon by the ion in an excited state. The experimental two-electron coincidence spectra obtained with both XUV and infrared radiation (Fig. 1 and Supplementary Fig. 1) exhibit features already present in Fig. 2b, albeit with modified intensity. In addition, new peaks appear throughout the spectrum and extend to higher total kinetic energy.

To understand the effect of the infrared field, we examine the difference between one-dimensional (1D) projections of spectra with and without infrared. In Fig. 3a we see a clear modulation

[1]Division of Synchrotron Radiation Research, Department of Physics, Lund University, Box 118, Lund 221 00, Sweden, [2]Division of Atomic Physics, Department of Physics, Lund University, Box 118, Lund 221 00, Sweden, [3]Department of Physics, Stockholm University, AlbaNova University Center, Stockholm 106 91, Sweden, [4]Research School of Physical Sciences, The Australian National University, Canberra, Australian Capital Territory 0200, Australia. *e-mail: mathieu.gisselbrecht@sljus.lu.se

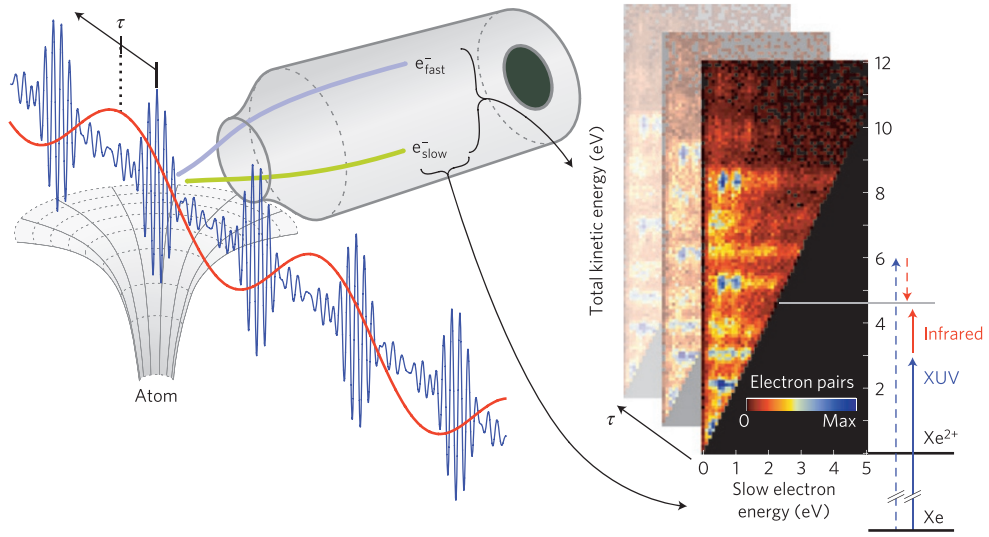

Figure 1 | Principle of the experiment. A xenon atom is ionized by an XUV attosecond pulse train in the presence of a weak infrared field, with photon energy 1.54 eV and intensity of 5×10^{11} W cm^{-2}. The electron energies are measured in a magnetic bottle electron spectrometer. The pressure and the XUV flux are chosen to detect an average of 0.07 electrons per laser shot. The experimental result is shown as a 2D coincidence spectrum. The colour indicates the probability of the electron pair as a function of the total and lowest kinetic energy of the pair, the latter denoted 'slow electron energy'. Such maps are recorded for different delays (τ) between the attosecond and infrared pulses. The energy diagram corresponding to our interferometric scheme is shown to the right for a final-state energy near 4.6 eV.

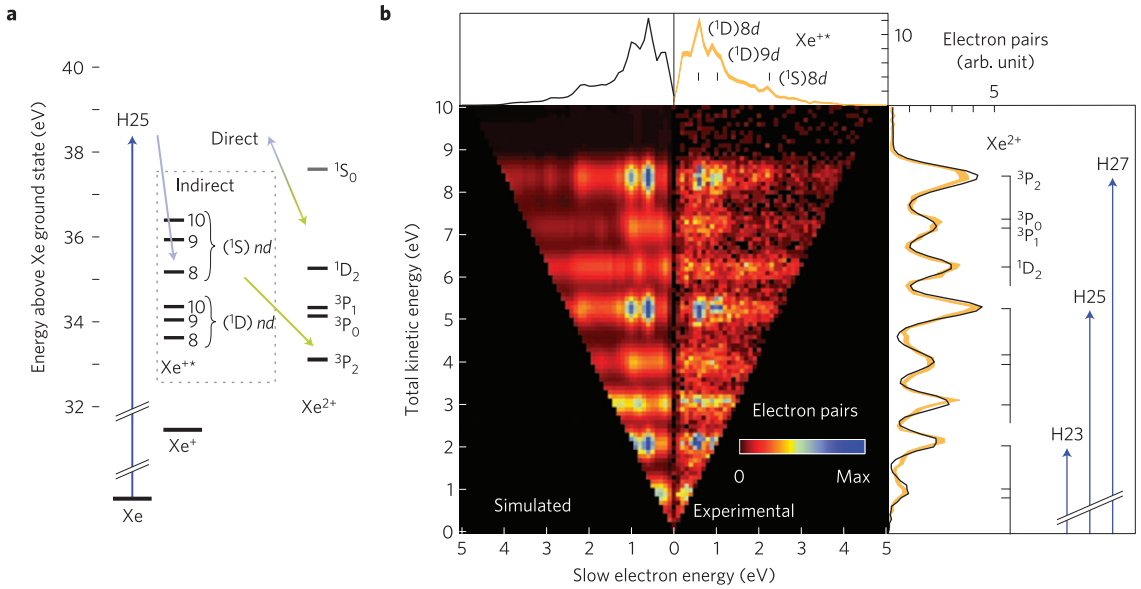

Figure 2 | Double ionization of Xe by attosecond pulse trains. a, Schematic energy level diagram in the vicinity of the double ionization threshold showing the XUV excitation and decay processes to the Xe^{2+} final states. The Xe^{2+} configuration has several multiplets spanning 4.5 eV due to strong spin–orbit splitting. Indirect single-photon DI occurs through autoionization of Xe^{+*} Rydberg states converging to the $^1S_0$ and $^1D_2$ states of Xe^{2+}. **b**, Measured two-electron coincidence spectra compared with simulated data (see Supplementary Methods). The electron pair spectrum contains stripes with constant total kinetic energy arising from different Xe^{2+} final states and harmonics 23, 25 and 27, as labelled on the projection on the total energy axis (rightmost panel). The projection on the slow-electron energy axis (top panel) shows peaks due to autoionization of Xe^+ $5p^4$ (^{1}D)*nd* and (^{1}S)*nd* to Xe^{2+} $^3P_2$. The thickness of the orange lines indicates the Poisson standard deviation of the data, while black lines represent the simulated spectra. Because we are using an attosecond pulse train (a frequency comb), the energy resolution is given by the harmonic bandwidth (~0.2 eV) for the total energy. For the slow energy, our resolution is given by the spectrometer (~50 meV).

of the projection on the total kinetic energy axis. DI peaks due to absorption of single harmonic photons (harmonic, H) are reduced whereas those due to two-colour DI (sidebands, SB) are enhanced. In Fig. 3b an enhancement of low-energy electrons induced by the infrared field is visible. The simulation including both sequential and non-sequential two-photon processes reproduces the projected experimental spectra very well. The non-sequential contribution accounts for the majority of the features seen in the projection on the total kinetic energy axis (Fig. 3a). The sequential contribution produces the low-energy peaks in the projection on the slow-electron energy axis (Fig. 3b) due to ionization from Xe^{+*} states lying within one infrared photon energy below the DI threshold. There is no experimental evidence for sequential processes via higher lying (autoionizing) Rydberg states.

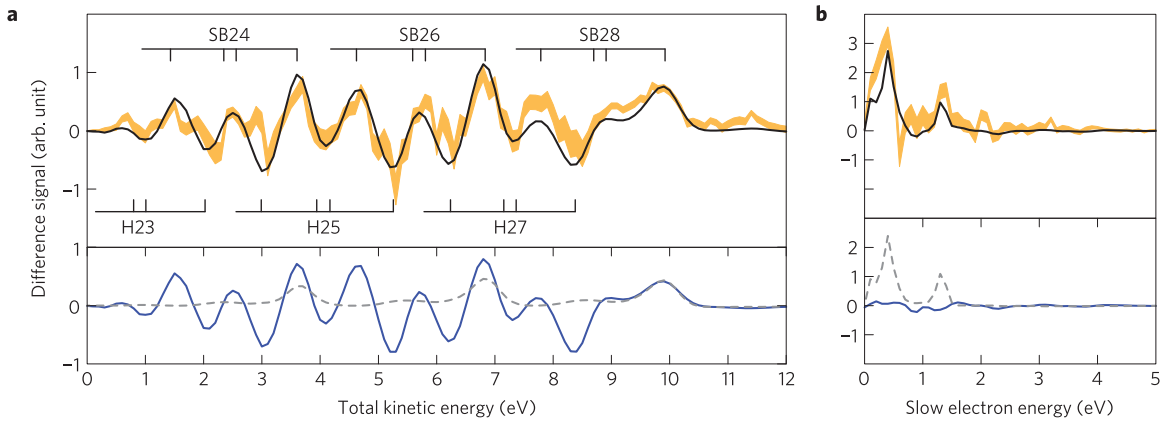

Figure 3 | Sequential and non-sequential double ionization. **a**,**b**, Difference of spectra obtained with and without the infrared field. Projections on the total kinetic energy (**a**) and the slow electron energy axes (**b**). The signal unit is the same as for the projections in Fig. 2. The experimental data (orange) are well reproduced by the full simulation (black). The contributions to the simulation can be broken into sequential (dashed grey) and non-sequential (solid blue) processes, which allows us to determine their respective contributions. The non-sequential absorption is responsible for the formation of sidebands in **a**, whereas sequential absorption due to one infrared-photon absorption from Xe^{+*} states leads to additional low-energy peaks in **b**. The peak at 1.3 eV in **b** is due to absorption from $5p^4$ (^{1}D)7*d* and the 0.4 eV-peak is attributed to (^{1}S)6*d* and (^{3}P)7*d*.

Summarizing our interpretation of the spectra, we find that xenon atoms in the presence of two (weak) XUV and infrared fields can be doubly ionized both through sequential and non-sequential processes. In contrast to previous studies using femtosecond light pulses[22], both of these contributions can be clearly identified in the two-electron coincidence spectrum (Fig. 1). The sequential process affects only the region below 1.5 eV for the slow electron whereas the non-sequential process dominates when the energies of the two electrons are similar. Final states can then be populated by two quantum paths: absorption of a harmonic and an infrared photon or absorption of the next harmonic and stimulated emission of an infrared photon, as shown in Fig. 1 (right). These two paths can interfere, indicating that the two-electron wave packet remains coherent during the measurement. The interference signal, which varies with the delay between the XUV and infrared pulses, carries the signature of the two-electron emission dynamics.

We concentrate our temporal study on non-sequential DI at a fixed total absorbed energy of 40.1 eV, corresponding to sideband 26. We choose this sideband to have a clear interferometric interpretation, because sideband 26 can be reached from below by harmonic 25 and from above by harmonic 27. Figure 4a shows the corresponding coincidence spectrum, with total kinetic energies 4.6 and 6.8 eV for ionization to the $^1D_2$ and $^3P_2$ states and in Fig. 4b presents the spectral regions where the signal oscillates as a function of the delay between the XUV and infrared fields. The colour-coded DI time delays are obtained by fitting the experimental data, as in Fig. 4e. The reference 'clock' is given by the Xe^+5p^{-1} single ionization signal recorded in the same experimental scan. In Fig. 4e, the DI delay relative to SI is $\tau_{DI}^{exp} - \tau_{SI}^{exp} = 55 \pm 61$ as. The uncertainty is much smaller than our measurable delay range, which is $\pm$ 670 as (half of the laser period).

A quantum mechanical description of SI time delays involved in attosecond interferometric experiments[6] (or similarly in streaking[8,23]) shows that the measured delay is the sum of two different contributions: the group delay of the electronic wave packet created by one-photon absorption (τ_{SI}^{1ph}), which contains information on the atomic potential, and the delay added by the interaction with the infrared field[24–26] (τ_{cc}). In general $\tau_{SI}^{1ph} = \partial \arg M / \partial E$, where M is the (complex) photoionization matrix element and E is the (total) kinetic energy (atomic units are used throughout). In the case of single ionization and a dominant non-interacting channel with a certain angular momentum, $\tau_{SI}^{1ph} = \mathrm{d}\eta/\mathrm{d}E$ is the so-called Wigner delay, equal to the derivative of the scattering phase η. It describes the dispersion of the electronic wave packet in the potential well, analogous to the group delay dispersion of a light pulse in a medium. The interaction with the infrared field results in a negative delay ($\tau_{cc} < 0$), which can be calculated analytically using asymptotic expressions for the continuum wave functions[26].

The theoretical description of double ionization is still an open problem, especially for complex systems such as xenon[27] and, to date, there is no formalism regarding the delay for the escape of the two electrons. In the present work, we establish using lowest-order many-body perturbation-theory (see Supplementary Methods) that the measured delay is equal to $\tau_{DI}^{1ph} + \tau_{cc}$, with

$$\tau_{DI}^{1ph} = \frac{1}{2}\left(\mathrm{d}\eta_1/\mathrm{d}E_1 + \mathrm{d}\eta_2/\mathrm{d}E_2\right) + \tau_{ee}$$

τ_{DI}^{1ph} is expressed as the average of the one-electron emission delays, E_1 and E_2 being the kinetic energies of the two emitted electrons, plus a correction term τ_{ee} describing the interaction between the two electrons. We calculate τ_{DI}^{1ph} using the random phase approximation with exchange[28] for the two fundamental direct DI mechanisms (shake-off and knockout, see Supplementary Methods). These time delays are positive, typically a few hundreds of attoseconds, and compensate those due to the interaction with the infrared field (τ_{cc}).

The results of our calculations are presented in Fig. 4c,d. The near synchronization between SI and DI observed in the experiment is supported in the calculations. For the particular case shown in Fig. 4e, we have $\tau_{DI}^{theo} - \tau_{SI}^{theo} = +80$ as for shake-off and $\tau_{DI}^{theo} - \tau_{SI}^{theo} = +5$ as for knockout. Our experimental result lies closer to the calculated value for the shake-off mechanism. In helium, shake-off can be described by taking the overlap between the neutral and ionic one-electron wavefunctions[11] (sudden approximation), but in xenon 5*s* and 5*p* inter-shell correlation effects must be included. Our analysis emphasizes the need for first-principles calculations to obtain a quantitative evaluation of the relative strength between shake-off and knockout and to include the influence of other mechanisms, for example DI via an indirect process[23].

In conclusion, we demonstrate that interferometric methods with attosecond pulses give us new insight into several aspects of DI (sequential/non-sequential, direct/indirect and shake-off/knockout). With further refinement of both attosecond sources at higher repetition rate and coincidence schemes, including for

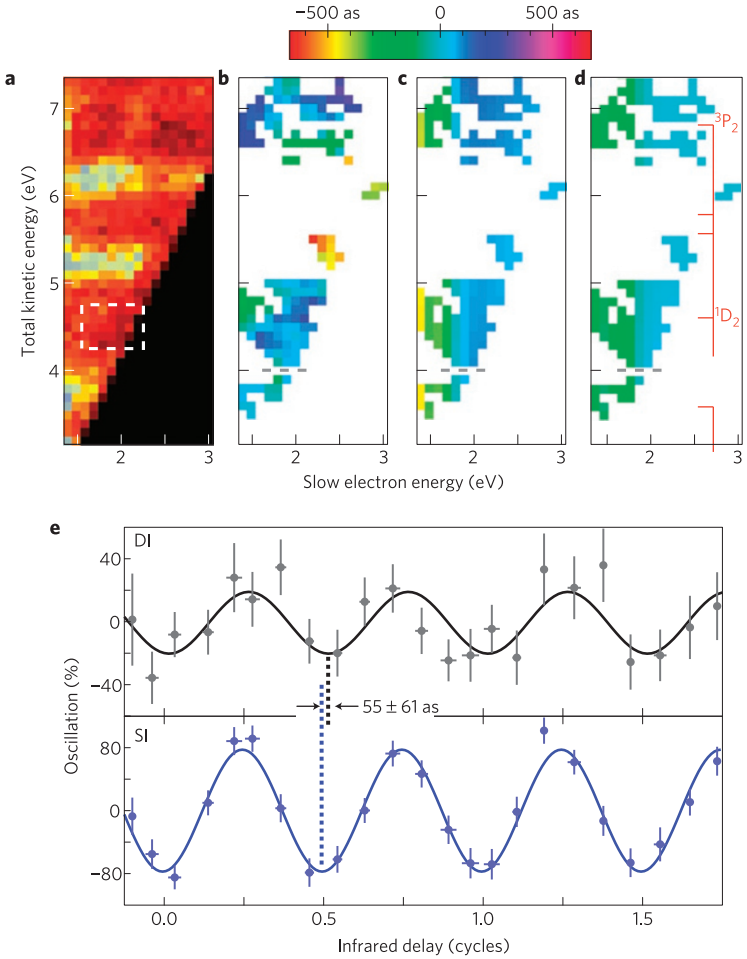

Figure 4 | Temporal study of double ionization. **a**, Electron pair spectrum corresponding to non-sequential DI. The colour scale is the same as in Fig. 2b. **b**, Experimental delays ($\tau_{DI}^{exp} - \tau_{SI}^{exp}$). Coloured areas indicate spectral regions where the signal oscillates in the experiment. **c**,**d**, Calculated delays ($\tau_{DI}^{theo} - \tau_{SI}^{theo}$) for the shake-off (**c**) and knockout (**d**) mechanisms with $\tau_{SI}^{theo} = -50$ as. The red labels on the right indicate the final ionic states corresponding to sideband 26 (above the dashed line) and sideband 24 (below the dashed line). **e**, SI and DI signals as a function of infrared delay. The DI signal is due to direct ionization to the $^1D_2$ state (dashed box in **a**). In the case of DI, the vertical error bar is statistical, corresponding to one-standard deviation for a Poissonian distribution, whereas for SI, it arises from fitting a sideband intensity profile to the photoelectron spectrum. Horizontal error bars show the standard deviation of raw data points between different scans. See Supplementary Methods for further details.

example angular resolution, our approach could be extended to the dynamics of more complex systems with potential applications in materials science[29] and biology[30].

Received 27 March 2013; accepted 19 December 2013; published online 26 January 2014

References

1. Briggs, J. S. & Schmidt, V. Differential cross sections for photo-double-ionization of the helium atom. *J. Phys. B* **33,** R1–R48 (2000).
2. Avaldi, L. & Huetz, A. Photodouble ionization and the dynamics of electron pairs in the continuum. *J. Phys. B* **38,** S861–S891 (2005).
3. Kheifets, A. S., Ivanov, I. A. & Bray, I. Timing analysis of two electron photoemission. *J. Phys. B* **44,** 101003 (2011).
4. Paul, P. M. *et al.* Observation of a train of attosecond pulses from high harmonic generation. *Science* **292,** 1689–1692 (2001).
5. Kienberger, R. *et al.* Atomic transient recorder. *Nature* **427,** 817–821 (2004).
6. Klünder, K. *et al.* Probing single-photon ionization on the attosecond time scale. *Phys. Rev. Lett.* **106,** 143002 (2011).
7. Eland, J. H. D. *et al.* Complete two-electron spectra in double photoionization: The rare gases Ar, Kr, and Xe. *Phys. Rev. Lett.* **90,** 053003 (2003).
8. Schultze, M. *et al.* Delay in photoemission. *Science* **328,** 1658–1662 (2010).
9. Goulielmakis, E. *et al.* Real-time observation of valence electron motion. *Nature* **466,** 739–743 (2010).
10. Mauritsson, J. *et al.* Attosecond electron spectroscopy using a novel interferometric pump–probe technique. *Phys. Rev. Lett.* **105,** 053001 (2010).
11. Schneider, T., Chocian, P. L. & Rost, J-M. Separation and identification of dominant mechanisms in double photoionization. *Phys. Rev. Lett.* **89,** 073002 (2002).
12. Schmidt, V. Photoionization of atoms using synchrotron radiation. *Rep. Prog. Phys.* **55,** 1483–1659 (1992).
13. Weber, T. *et al.* Correlated electron emission in multiphoton double ionization. *Nature* **405,** 658–661 (2000).
14. Pfeiffer, A. N. *et al.* Timing the release in sequential double ionization. *Nature Phys.* **7,** 428–433 (2011).
15. Kikas, A. *et al.* High-resolution study of the correlation satellites in photoelectron spectra of the rare gases. *J. Electron Spectrosc. Relat. Phenom.* **77,** 241–266 (1996).
16. Alitalo, S. *et al.* The valence photoelectron satellite spectra of Kr and Xe. *J. Electron Spectrosc. Relat. Phenom.* **114–116,** 141–146 (2001).
17. Laulan, S. & Bachau, H. Correlation effects in two-photon single and double ionization of helium. *Phys. Rev. A* **68,** 013409 (2003).
18. Feist, J. *et al.* Probing electron correlation via attosecond XUV pulses in the two-photon double ionization of helium. *Phys. Rev. Lett.* **103,** 063002 (2009).
19. De Morisson Faria, C. F. & Liu, X. Electron electron correlation in strong laser fields. *J. Mod. Opt.* **58,** 1076–1131 (2011).
20. Horner, D. A., Morales, F., Rescigno, T. N., Martín, F. & McCurdy, C. W. Two-photon double ionization of helium above and below the threshold for sequential ionization. *Phys. Rev. A* **76,** 030701 (2007).
21. Rantovic, P. *et al.* Laser-enabled Auger decay in rare-gas atoms. *Phys. Rev. Lett.* **106,** 053002 (2011).
22. Guyétand, O. *et al.* Complete momentum analysis of multiphoton photo-double ionization of xenon by XUV and infrared photons. *J. Phys. B* **41,** 065601 (2008).

23. Pazourek, R., Feist, J., Nagele, S. & Burgdörfer, J. Attosecond streaking of correlated two-electron transitions in helium. *Phys. Rev. Lett.* **108,** 163001 (2012).
24. Guénot, D. *et al.* Photoemission-time-delay measurements and calculations close to the 3s-ionization-cross-section minimum in Ar. *Phys. Rev. A* **85,** 053424 (2012).
25. Ivanov, M. & Smirnova, O. How accurate is the attosecond streak camera? *Phys. Rev. Lett.* **107,** 213605 (2011).
26. Dahlström, J. M., L'Huillier, A. & Maquet, A. Introduction to attosecond delays in photoionization. *J. Phys. B* **45,** 183001 (2012).
27. Yip, F. L., Rescigno, T. N., McCurdy, C. W. & Martín, F. Fully differential single-photon double ionization of neon and argon. *Phys. Rev. Lett.* **110,** 173001 (2013).
28. Amusia, M. Y. *Atomic Photoeffect* (Plenum Press, 1990).
29. Schnadt, J. *et al.* Experimental evidence for sub-3-fs charge transfer from an aromatic adsorbate to a semiconductor. *Nature* **418,** 620–623 (2002).
30. Harbach, P. H. P., Schneider, M., Faraji, S. & Dreuw, A. Intermolecular coulombic decay in biology: The initial electron detachment from $FADH^-$ in DNA photolyases. *J. Phys. Chem. Lett.* **4,** 943–949 (2013).

Acknowledgements

We thank A. Maquet and R. Taïeb for fruitful theoretical discussions. This research was supported by the Marie Curie program ATTOFEL (ITN), the European Research Council (ALMA), the Swedish Research Council and the Knut and Alice Wallenberg Foundation.

Author contributions

E.P.M., D.G., C.L.A., D.K., S.K. and M.G. performed the experiment. E.P.M., J.M.D., E.L., A.S.K., D.G., A.L. and M.G. worked on the analysis and theoretical interpretation. E.P.M., S.L.S., A.L. and M.G. wrote the manuscript.

Additional information

Supplementary information is available in the online version of the paper. Reprints and permissions information is available online at www.nature.com/reprints. Correspondence and requests for materials should be addressed to M.G.

Competing financial interests

The authors declare no competing financial interests.